Emergence and Interpretation of Oscillatory Behaviour Similar to Brain Waves and Rhythms*

Javier A. Galadí[a,1,3], Joaquín J. Torres[a,2,3,*], J. Marro[a,2]

[a] *Institute "Carlos I" for Theoretical and Computational Physics, University of Granada, Granada, Spain.*

Abstract

Electroencephalography (EEG) monitors —by either intrusive or noninvasive electrodes— time and frequency variations and spectral content of voltage fluctuations or waves, known as *brain rhythms*, which in some way uncover activity during both rest periods and specific events in which the subject is under stimulus. This is a useful tool to explore brain behavior, as it complements imaging techniques that have a poorer temporal resolution. We here approach the understanding of EEG data from first principles by numerical simulating and studying a networked model of excitatory and inhibitory neurons which generates a variety of comparable waves. In fact, we thus numerically reproduce oscillatory behavior similar to α, β, γ and other rhythms as observed by EEG recordings, and identify the details of the respectively involved complex phenomena, including a precise relationship between an input and the collective response to it. It ensues the potentiality of our model to better understand actual brain oscillatory activity in normal and pathological situations, and we also describe kind of *stochastic resonance* phenomena which could be useful to locate main qualitative changes of brain activity in (e.g.) humans.

Keywords: EEG numerical simulation, Brain phase transitions, Brain activity stochastic resonance.

*All authors equally contributed to write the manuscript.

*Corresponding author: jtorres@onsager.ugr.es

[1]Current Address: Department of Differential Equations and Numerical Analysis, University of Seville, Spain.

[2]These authors proposed and designed the research.

[3]These authors wrote the codes and performed the simulations.

Introduction

There has been a growing interest in investigating the occurrence of phenomena associated with thermodynamic-like phase transitions and criticality during the functioning of neural media by means of novel experimental techniques, analysis of available connectome data, and numerical simulations of biological-inspired theoretical approaches; see, e.g., [1, 2, 3, 4, 5, 6], and references therein. In particular, a sort of brain critical behavior —mimicking essential features of phase transition phenomena such as condensation and ferromagnetism— is now believed to be at the origin of the observed good processing throughout the brain of signals coming from different areas and the senses [7, 8, 6, 9]. That is, there has recently emerged definite evidence that weak signals are optimally transferred and even enhanced in a noisy environment when the system is in a well-defined region with great susceptibility which happens to separate neuron dynamic "phases", i.e., areas in parameter space in which the brain shows qualitatively different kinds of behavior [3, 5]. Ref. [3] also presents a feasible procedure to experimentally detect phase transitions and their details during the performance of actual brains. Following this promising path, in the present paper we investigate the possibility of visualizing phase transitions during brain operation by using easily-extracted brain-activity data obtained from EEG (by the same token, magnetoencephalograph) recordings. It ensues what we hope is a convenient tool to monitor *in vivo* changes between different dynamic behaviors of the cerebral activity. It may also follow how to design specific stimuli to control these dynamic phases and eventually modify some of their properties, e.g., in cases of dysfunction.

More specifically, we here present, numerically simulate and discuss an EEG neural-activity model, which generalizes and formalizes a previous one [10]. We link this to a familiar mathematical framework, improve the temporal precision of the original setting (using a time step of 40 millionths of a second), include an appropriate tuning of the noise, and consider the possibility of an input signal that makes the model useful to reveal and analyze new intriguing phenomena. This increase in the model temporal integration precision ensures avoiding artifacts, such as non-real synchronicity, in particular for high intensity noisy inputs. In addition, our model also includes two basic realistic assumptions concerning the cortical activity in the human

brain as Excitation/Inhibition balance [11] and the relation of the intrinsic noise with a noisy input to each neuron in the network that mimics the excitatory activity from other brain areas that project into our system.

The new setting allows us to deep on how oscillation patterns, e.g., as observed by electroencephalography, emerge reflecting different dynamic activity, and we thus infer the precise role of the intrinsic noise in causing some familiar rhythms in the human brain. It ensues that not only α rhythms but also β, γ and ultrafast oscillations are all just a form (at different levels) of the same "noise" as it is *filtered* (in a way that our model clarifies) by the neural network itself. More precisely, we demonstrate here that in a realistic modeled brain module that receives a Poissonian noise input in which there is not a defined frequency, only its intensity, the collective behavior of the brain module is an oscillation with a well-defined frequency (which characterized the corresponding brain rhythm) and that this frequency depends on the intensity of the input noise. That is, one may conclude that the cause for brain waves is universal within this context, which allows us to consider a unique mechanism for any of the mentioned voltage fluctuations with only a relevant parameter. This, we show, is the intensity of the sum of all the inputs, either noisy or constant, reaching the network from the outside, and we succeed in parameterizing it. Consequently, we are able to rigorously relate the occurrence of phase transitions —actually, having a non-equilibrium nature [12, 5]— in the brain with different possible dynamic behaviors which are revealed by the easily-observed EEG rhythms mentioned. It is with this aim that we here use and numerically simulate a network, which involves both excitatory and inhibitory units, where a random input is sufficient to generate different brainwaves, some of them respectively corresponding to α, β, γ and ultrafast oscillations. We also precisely relate the intensity of the input and the frequency of the resulting dynamic response and —following a method first reported in [3]—we show how to use an external signal in a simple experiment to identify the undergoing phase changes and other details during brain operation using the well known mechanism of stochastic resonance (SR) [13]. The close relation between the oscillatory emergent behavior in our system and actual brain waves as those observed, for instance, in EEG recordings, suggests that the same SR experiments to detect phases transitions can be visualized in actual brains designing, for instance, appropriate pychophysical experiments that show a high susceptibility of the brain activity to given stimuli in the presence also of noisy inputs.

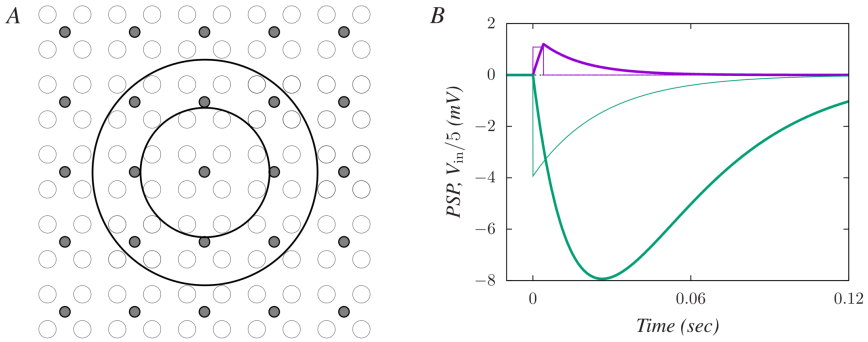

Figure 1: Model features. Left panel: a portion of the actual network topology (we here in practice considered $N = 180$ nodes), where filled circles stand for inhibitory (I) neurons and open circles represent excitatory (E) neurons. In order to mimic biological conditions (and following [10]), the largest of the two concentric circles drawn includes 32 Es which influence the I at its center, and the smallest concentric circle includes 12 Es under the influence of that I. Right panel: an excitatory postsynaptic potential (EPSP; topmost, purple curve) and an inhibitory one (IPSP; lowermost, green curve) as modeled using the time-dependent voltage functions $V^E(t)$ and $V^I(t)$ (see main text) for parameter values in [10], namely, $t_{\max} = 4\,ms$, $\epsilon = 0.3425\,V/s$, $\eta = -0.82\,V/s$, $\tau_1 = 16\,ms$ and $\tau_2 = 26.3\,ms$. For illustrative purposes, we also show here (with thinner lines) the two functions in Eq. (2).

Model and method

Consider, for simplicity and ease of representation, a regular two-dimensional network on a torus —in which periodic boundary conditions avoid surface effects and simulate a larger system— with N nodes each holding either an *excitatory* (E) or an *inhibitory* (I) neuron as depicted in Fig. 1. They interact with each other such that any E excites one or more Is as long as the membrane voltage of the former exceeds a given threshold potential, and when any I exceeds its own threshold it will inhibit a group of Es (negative feedback). No delays are considered, which might exclude very extensive networks, and we also neglect both positive feedback of Es (any E stimulating another E) and negative feedback of Is (any I inhibiting other I). Furthermore, according to histological data —showing that, in portions of the cortex, there are about four times more excitatory than inhibitory neurons [14, 15, 16, 17]— the E/I ratio is assumed here to be 4, so that any I neuron receives effective excitatory inputs from 32 surrounding Es and any I neuron projects upon 12 surrounding Es, as illustrated in Fig. 1A.

For simplicity, we also assume that the EEG signal is an extracellular reflection of the sum of the membrane potentials of the neurons in our network, since synaptic events may propagate over large distances in extracellular space and be recordable as far as on the surface of the scalp, where they participate to the genesis of the EEG.

Dynamics

Each neuron is fully characterized by a potential or "voltage membrane" V which evolves in time —below a given threshold for firing, V_{th}— according to a type of integrate-and-fire dynamics [18] under various contributions, namely,

$$\tau \frac{dV(t)}{dt} = -V(t) + V_{\text{in}}(t) + V_{\text{ext}}(t) + V_{\text{noise}}(t) + V_0, \tag{1}$$

where $V_0 = RI_0$ is a constant voltage term induced by a constant current I_0 (so that R characterizes the neuron membrane resistance), and V_{ext} stands for an external well-defined signal that we in practice implement as a sinus (in order to trace it easily). These compete with a noise V_{noise}, which corresponds to uncorrelated depolarizing signals from other areas of the brain, and we assume here that such excitatory inputs occur at times that are Poisson distributed with mean μ. This, which also characterizes the noise distribution broadness, will be used as a principal parameter in our study. Furthermore, a main contribution in (1) is the total signal V_{in} arriving to the given neuron from its presynaptic (neighbor) neurons. In order to take phenomenological account of the observed dynamic behavior of synaptic connections [3], we assume this may be written, for a single presynaptic excitatory or inhibitory input, as (cf. thin lines in Fig. 1B)

$$V_{\text{in}}(t) = \begin{cases} \epsilon\tau \left[\Theta\left(t - t_{\text{in}}\right) - \Theta\left(t - t_{\text{in}} - t_{\max}\right)\right] & \text{depolarizing inputs} \\ \eta\tau\Theta\left(t - t_{\text{in}}\right)\exp\left[-\left(t - t_{\text{in}}\right)/\tau\right] & \text{hyperpolarizing inputs.} \end{cases} \tag{2}$$

Here, t_{in} is the time at which the presynaptic input occurs, the first line is for the excitatory input of amplitude $\epsilon\tau$ and duration $t_{\max}$ arriving to the neuron, and the second line stands for the exponentially-decaying inhibitory input (decreasing η per unit time). $\Theta(X)$ is the Heaviside step function.

For $V_0 = V_{\text{ext}} = V_{\text{noise}} = 0$, one may prove by exact integration of (1) with (2) that the induced depolarizing and hyperpolarizing waves generated by a single input from an excitatory neuron and an inhibitory presynaptic

one are, respectively,

$$V^E(t) = \begin{cases} 0 & t \leq t_{\text{in}} \\ \epsilon\tau_1 \left\{1 - \exp\left[-(t - t_{\text{in}})/\tau_1\right]\right\} & t_{\text{in}} < t \leq t_{\text{in}} + t_{\max} \\ \lambda \exp\left[-(t - t_{\text{in}} - t_{\max})/\tau_1\right] & t > t_{\text{in}} + t_{\max} \end{cases} \tag{3}$$

and

$$V^I(t) = \begin{cases} 0 & t \leq t_{\text{in}} \\ \eta(t - t_{\text{in}}) \, \exp\left[-(t - t_{\text{in}})/\tau_2\right], & t > t_{\text{in}}, \end{cases} \tag{4}$$

where $\lambda \equiv V^E\left(t_{\text{in}} + t_{\max}\right) = \epsilon\tau_1\left[1 - \exp\left(-t_{\max}/\tau_1\right)\right]$ and $\tau_1\left(\tau_2\right)$ is τ in (2) for excitatory (inhibitory) inputs. That is, the absolute values of $V^E(t)$ and $V^I(t)$ decay exponentially towards a membrane rest value after a time $t = t_e$ — being $t_e = t_{\text{in}} + t_{\max}$ for $V^E(t)$ and $t_e \approx t_{\text{in}} + 0.06$ for $V^I(t)$ — with respective characteristic times τ_1 and τ_2. These functions are illustrated in panel B of Fig. 1. The values for the parameters η, ϵ and τ appearing in (2) has been taken (see the caption of Fig. 2B) such that the corresponding depolarizing and hyperpolarizing waves in (3) are biologically realistic. Small variations of these values, however, have not a strong influence in the emergent behavior of the system (data not shown).

In order to reproduce the antecedent in [10] from this formalization, one needs to discretize the above continuous dynamics by defining instants $t_i = i\Delta t$, $i = 1, \ldots, n$, with Δt a time interval, which we assume to be $\Delta t = 40\,\mu s$ in practice. We then obtain from (1), for $V_0 = V_{\text{ext}} = V_{\text{noise}} = 0$ and denoting $V_i = V(t_i)$, that this discretely evolves under the action of a the depolarizing and hyperpolarizing inputs, respectively, as

$$V_{i+1} = \begin{cases} a_E V_i + \epsilon\Delta t \, \left[\Theta\left(i - i_{\text{in}}\right) - \Theta\left(i - i_{\text{in}} - i_{\max}\right)\right] \\ \\ a_I V_i + \eta\Delta t \, \Theta\left(i - i_{\text{in}}\right) \exp\left[-\left(i - i_{\text{in}}\right)\left(1 - a_I\right)\right] \end{cases} \tag{5}$$

where $a_E = 1 - \Delta t/\tau_1$, $a_I = 1 - \Delta t/\tau_2$ and i_{in} is the time step at which the presynaptic hyperpolarizing pulse occurs, that is, $t_{\text{in}} = i_{\text{in}}\Delta t$ and $i_{\max} = t_{\max}/\Delta t = 100$. One may generalize this expression to the cases of a train of m depolarizing or hyperpolarizing pulses at temporal points $i_1, \ldots, i_m$ by writing, respectively:

$$V_{i+1} = a_E V_i + \epsilon\Delta t \sum_{k=1}^{m} \left[\Theta\left(i - i_k\right) - \Theta\left(i - i_k - i_{\max}\right)\right], \tag{6}$$

$$V_{i+1} = a_I V_i + \eta \Delta t \sum_{k=1}^{m} \Theta\left(i - i_k\right) \exp\left[-\left(i - i_k\right)\left(1 - a_I\right)\right]. \tag{7}$$

It should be noted here that several, either depolarizing or hyperpolarizing, waves can occur at the same time step. Also noticeable is that the first terms in these two equations correspond to the final exponential decreases in absolute value toward the resting value of V after the last depolarizing or hyperpolarizing pulses with characteristic time constants a_E and a_I, respectively. Following [10] to prevent that during numerical simulations the sum of depolarizing pulses in the second term of (6) makes the voltage V_i to overpass its maximum value V_{sat}, we introduced a factor $\left(V_{\text{sat}} - V_i\right)/V_{\text{sat}}$ multiplying this term. Likewise, to prevent that the sum of hyperpolarizing pulses in the second term of (7) makes V_i to go below its minimum V_{min}, we introduced a factor $\left(V_{\text{min}} - V_i\right)/V_{\text{min}}$. The resulting final dynamics for a given neuron will depend on whether such neuron is E or I. Thus, for E neurons, which receive both, depolarizing and hyperpolarizing pulses respectively from E and I presynaptic neurons, the final dynamics becomes

$$\begin{aligned} V_{i+1} = a V_i &+ \frac{V_{\text{sat}} - V_i}{V_{\text{sat}}} \sum_{k=1}^{m} \epsilon \Delta t \left[\Theta\left(i - i_k\right) - \Theta\left(i - i_k - i_{\max}\right)\right] \\ &+ \frac{V_{\text{min}} - V_i}{V_{\text{min}}} \sum_{k=1}^{l} \eta \Delta t\, \Theta\left(i - i_k\right) \exp\left[-\left(i - i_k\right)\left(1 - a_I\right)\right] \end{aligned} \tag{8}$$

where $a = a_E$ or a_I depending on whether the potential V_i after the last received pulse is either above or below V_{rest}. On the other hand, for I neurons which receive only depolarizing pulses from their presynaptic E neurons, the final dynamics becomes

$$V_{i+1} = a_E V_i + \frac{V_{\text{sat}} - V_i}{V_{\text{sat}}} \sum_{k=1}^{m} \epsilon \Delta t \left[\Theta\left(i - i_k\right) - \Theta\left(i - i_k - i_{\max}\right)\right]. \tag{9}$$

Note that (1) involves the usual re-scaling $V(t) \to V(t) + 60\, mV$ of the membrane potential in actual neurons [22] in order to get the neurons membrane potential in the resting state $V_{\text{rest}} = 0\ mV$, instead of $V_{\text{rest}} = -60 mV$. Then, the time evolution in (8) and (9) is also conditioned by the fact that the neurons membrane potential is not allowed either to decrease in the course of hyperpolarization below $V_{\text{min}} = -20\, mV$ nor exceed the saturation level

$V_{\text{sat}} = +90\,mV$, both limits within the known physiological range. Concerning the model dynamics (8) for E neurons, note also that the first sum of its right-hand side is such that the times $t_k = i_k \Delta t\,(k = 1, ..., m')$ at which the depolarizing (excitatory) inputs arrive to these neurons from outside the network are Poisson distributed; such term corresponds to V_{noise} (see below). Likewise, the second sum in (8) corresponds in this case to inputs from I neurons that fire at times $t_k = i_k \Delta t$ $(k = 1, \ldots, l)$ since E neurons only receive inputs from inhibitory neurons in our network. On the other hand, in the case of I neurons, the sum in the right-hand side of (9) corresponds to contributions from Es in the network that fire at times $t_k = i_k \Delta t$ $(k = 1, \ldots, m)$ since I neurons only receive inputs from Es in the network and are isolated from the outside.

Inputs

The inputs V_{ext}, V_{noise} and V_0 arrive only to the E cells since the Is play the role in the model of communication bridges among Es. In particular, we consider only non-relay interneurons, i.e., local ones (with short dendrites and axons) that receive inputs from proximal neurons but never from distant parts of the brain [19]. Therefore, the Is are isolated from external influences.

Also, trying to reflect better reality, during numerical simulations of the model it is assumed that V_{noise} is a randomly distributed series of independent and uncorrelated in space and time EPSPs corresponding to depolarization waves as given by (3), and that the E cells are the only ones that receive such noisy input. Our choice for this noise is based on reports showing that often these series of action potentials are Poisson distributed [20, 21]. The noise level parameter μ represents the mean value of action potentials in one hundred time steps and per cell, i.e., each excitatory cell receives on average $\lambda = \mu/100$ depolarization waves from outside per unit time. Then, to numerically simulate a Poisson distribution of inputs with mean λ, we assume that each E receives random inputs from n external neurons with probability λ/n of firing per time step with n large enough so that such binomial distribution becomes a Poissonian one.

On the other hand, the stimulus V_{ext} does not in general refer to a sensory stimulus, given that our system can be interpreted as a small brain module with just a few hundred neurons, and V_{ext} may have electrochemical contributions from neurons outside that module.

Firing threshold

The main physiological properties of E and I neurons are here assumed to be the same. In particular, following known facts [22], the firing threshold of both are set at $V_{\rm th}$ ($= 6\,mV$ in practice) above the resting membrane potential and, after firing, the threshold is changed to $V_{\rm sat}$ in order to numerically simulate the absolute refractory period during one hundred time units ($t_a = 4\,ms$). Also, to simulate the relative refractory period once the absolute refractory period lasts, we consider that the threshold value decreases exponentially. That is, after firing an action potential at t_f we have

$$V_{\rm th}(t) = \begin{cases} V_{\rm sat} & t_f < t < t_f + t_a \\ 6 + (V_{\rm sat} - 6)\exp\left[-\kappa\,(t - t_f - t_a)\right] & t_f + t_a < t. \end{cases}$$

Here, a good fit to the typical threshold stimulus strength required to elicit an action potential during the relative refractory period is achieved, for example, with $\kappa = 2\,ms^{-1}$. This assumption in our model differs from the standard integrate-and-fire models [18] which assume a constant $V_{\rm th}$, reset the membrane voltage at $V_{\rm rest}$ during the absolute refractory period, and assume lack of a relative refractory period.

Results

We monitored several dynamic variables during numerical simulations of the network evolution with time, including: (a) the average of membrane potentials (reversing their re-scaling, i.e., $V(t) \to V(t) - 60\ mV$ for a more realistic physiological illustration) of E neurons; (b) the same for I neurons; and (c) the action potentials density leaving the network via axons or the fraction of firing E neurons at time t, i.e., $\rho(t) = (1/N_E)\sum_{i=1}^{N_E} s_i^E(t)$ where $s_i^E(t) = 1, 0$ if the E neuron is firing or not at time t. Since the number of Es is dominant, we identify (a) with the EEG signal which, therefore, is assumed to be the extracellular replica of the membrane time variation. This is a sensible assumption since EEG experiments are expected to record at a site on the scalp the summed electrical field potentials from all cortical neurons in a certain volume of tissue under the electrode. The fact is that a control of these quantities shows that the model steady state is quickly attained —typically in around $100\Delta t$ steps during our studies— from any initial condition. Although it will be more realistic to include also in the average (a) the membrane potentials of the I neurons (in fact an EEG electrode can detect E and I

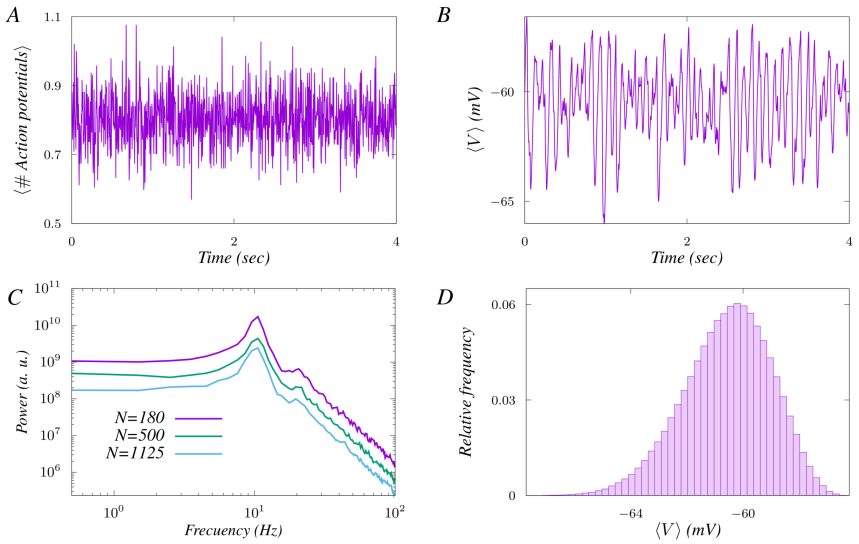

Figure 2: (A) Example of the noisy time series that each E neuron receives on the average from $n = 100$ external E neurons from outside the network. This has a Poisson distribution of mean $\mu = 0.8$. In practice, we compute the number of external action potentials each E neuron receives each time step $t_i = i\Delta t$ from such distribution, and add this number to the number of depolarization waves in the sum appearing in (8). (B) Emergent output of a network with $N = 180$ neurons as measured by the average membrane potential of all the E neurons. Its statistical features are shown in panels (C), depicting the sharp power spectral density and its dependence with the number of the neurons in the network, and (D), the corresponding probability distribution computed also for $N = 180$. Note in C, that although the power of the peak decreases as N increases, the noise power is also decreased, so the signal-to-noise ratio (SNR) remains the same independently of N. The same dependence with N occurs for all other values of the noise parameter, see e.g., Fig. 1 of Supplementary Information for $\mu = 0.6$.

membrane potentials), their main effect will be the appearance of a delayed phase and perhaps very small amplitude variations in the resulting oscillatory wave.

Consider first the case in which $V_{\text{ext}} = V_0 = 0$ (and therefore $I_0 = 0$) so that the only input in Eq. (1) besides V_{in} is V_{noise}. When this is implemented as a Poisson distribution, our system responds, as illustrated in Fig. 2, with a well-defined rhythm wave, in spite of the wide range of frequencies in the input, in agreement with experiments. That is, for a sufficiently large input mean ($\mu = 0.8$ in the example of Fig. 2) the two populations (E and I) of neurons show coupled oscillations producing collective coherent resonance,

and the familiar α-rhythm emerges. This is revealed, for instance, by the power spectral density of the time series for the average membrane potential over all E neurons, depicted in Fig. 2B, which shows a well-defined peak around 10.5 Hz in Fig. 2C. It is remarkable that increasing the network size does not alter significantly the emergence of the α-rhythm and its features as it is illustrated in Fig. 2C. In Fig. 2D is also illustrated that the steady state of the average membrane potential of all E neurons has a distribution centered around $V_{\rm rest} = -60\ mV$ that shows, for $\mu = 0.8$, slightly more frequent deviations to lower values produced by the IPSPs than deviations to higher values produced by the EPSPs of the noisy input.

There are indications that the same simple model may generate other types of rhythms as one varies the parameter μ. Would this be the case, it would generalize the last observation, already reported in [10], along an important path as it would indicate that all the familiar *brain-rhythms* may be considered as noise filtered by the networked system. As a matter of fact, decreasing μ we observe that the coupling between the two populations of neurons which induces the coherent rhythm tends to get worse. For instance, the time series of the mean membrane potential for $\mu = 0.6$ do not have the well defined periodicity nor, therefore, the acute peak in the power spectral density in Fig. 2C (see also Fig. 1 in Supplementary Information). We shall demonstrate below that such lack of periodicity for $\mu \sim 0.6$ corresponds to a phase transition between an incoherent oscillatory condition and a coherent one. This fact does not show up in [10] where a (one hundred times) larger time discretization artificially increases coherence —the same also obscures other important facts concerning larger values of μ, as we shall illustrate below.

The new circumstance uncovered here suggested us using μ as a control parameter, and thus explore further the emergence of brain rhythms, which then happen to surface as characteristics of *dynamic phases*. Fig. 3 partially illustrates the varied collective behavior that shows up as μ is increased adiabatically in time. This reveals that, following a rather disordered phase (I) for $\mu \lesssim 0.6$, oscillations become well defined (phase II) after $\mu \approx 0.6$. (see also Fig 2 of Supplementary Information for $\mu = 0.9$ where the power spectrum depicts a very sharp and clear peak at a given frequency). As μ is increased further, coherence is observed to decrease, as well as the synchrony within E and I populations —in particular, we observe that E neurons are

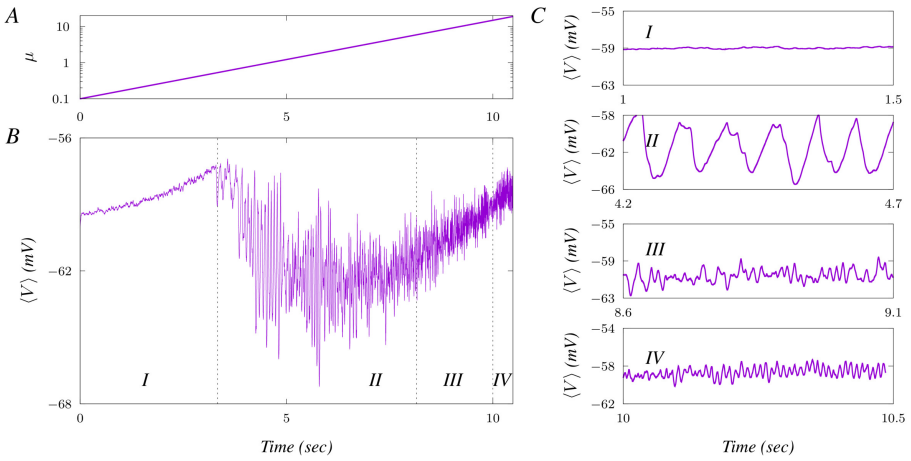

Figure 3: Some characteristics of the different dynamical phases that emerge as μ is varied. Panel A shows the (linear) adiabatic temporal variation of μ during the experiment, from $\mu = 0.1$ increasing by a factor 1.00002 every time unit Δt. The resulting dynamic behavior is illustrated in panel B showing $V(t)$, and this is detailed in panel C (right) for constant μ (=0.2, 0.9, 10 and 17, respectively) within the four regions of different behavior. Note how oscillations are too weak for $\mu \lesssim 0.6$ (phase I) to speak about actual coherence resonance, while they are clear for $\mu \gtrsim 0.6$, and coupling is observed best around $\mu = 1.5$. Thereafter, coherence begins to decrease and the synchronization within the E and I populations decreases. Between $\mu \approx 6$ and $\mu \approx 16$ there is an incoherent phase (III) in which frequency cannot be defined. However, coherence and synchrony within E and I populations are restored and the frequency is well-defined again for $\mu \gtrsim 16$ (phase IV).

first triggered simultaneously, which induces firing of Is at the same frequency but after a certain time lag. Incoherence then sets in from $\mu \approx 6$ to $\mu \approx 16$ (phase III), which induces an incoherent phase with no collective well-defined frequency (see also Fig. 2 of Supplementary Information that shows a plateau of frequencies for $\mu = 10$ without a clear peak in its power spectrum). However, coherence and synchrony within neuron populations with a clear collective frequency are restored for $\mu \gtrsim 16$ (phase IV) (see also Fig. 2 of Supplementary Information for $\mu = 17$ where a clear sharp peak at high frequency emerges in its power spectrum) until $\mu > 25$, when the noise is so high that it looses any biological meaning.

To confirm these —non-equilibrium but thermodynamic-like [12]— phases, instead of slowly varying μ we also maintained the noise constant during each simulation. Repeating this operation for different noise values of μ, we obtained the graphs in Fig. 3 which happen to illustrate different types of

behavior. In summary, we may define:

Phase I, $\mu \lesssim 0.6$: Incoherence phase with low spiking activity. The two subpopulations of neurons act almost uncoupled with no well-defined oscillation frequency.

Phase II, $0.6 \lesssim \mu \lesssim 6$: Synchronous activity in both E and I neuron populations with broad collective oscillations of the two subpopulations, which then coherently oscillate coupled at a well-defined frequency.

Phase III, $6 \lesssim \mu \lesssim 16$: High spiking activity with lost of the overall coherence. Ups and downs in the average membrane potentials of the two subpopulations are such that the excitation does not "wait" for the end of the inhibition in every period and vice-versa, so that the periodicity and rhythm that characterize phase II is now lost.

Phase IV, $\mu \gtrsim 16$: Highly synchronous activity within E and I neuron populations, namely, all the Es are triggered almost simultaneously, and the same with the Is. This is because the threshold is exceeded again in a short time (after each firing event and its subsequent refractory period) which facilitates synchronicity (and reduces the possibility of other type of behavior). This highly synchronous behavior goes with coherent oscillations of the average membrane potential with an amplitude lower than in phase II but is more regular than these and shows a well defined oscillation frequency, as revealed by the power spectrum.

It ensues that the familiar brain rhythms, namely, α, β, γ and ultrafast oscillations in EEG recordings from actual awake brains, have a well-defined correspondence with these rhythmic oscillations of the average membrane potential in the model. To clearly uncover this, we performed extra runs lasting 2^{18} time steps (equivalent to 10.5 s) for each of the 66 μ values in a geometric progression starting at $\mu = 0.5$. From such time series, we collected both the average membrane potential and the fraction $\rho(t)$ of firing E neurons in the population, then computed the power spectra for both signals, and searched for a maximum peak on each of them. Our main results are summarized in Fig. 4 where panel A depicts the frequency at which this maximum peak occurs as a function of μ. There is no evidence of any well defined frequency with a maximum peak for $\mu \lesssim 0.6$ (phase I, not shown), nor for $6 \lesssim \mu \lesssim 16$ (phase III) which shows abrupt jumps. However, such

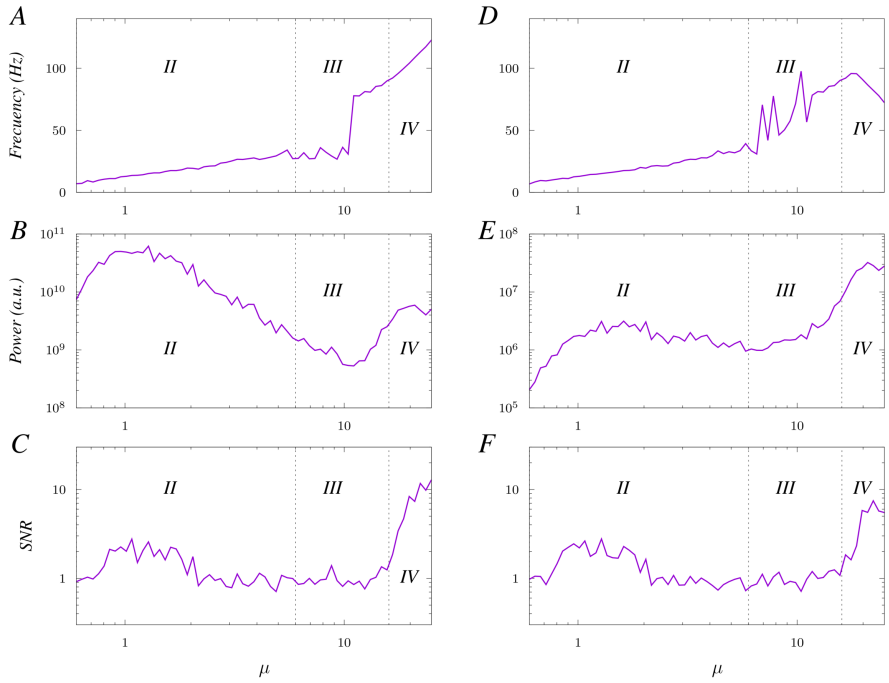

Figure 4: Panel A: Frequency at the power spectra peak of time series for the mean membrane potential as a function of μ for $I_0 = 0$. There is asynchrony within E and I neuron populations resulting in an incoherent oscillatory behavior for $6 \lesssim \mu \lesssim 16$ (phase III) and regions of coherence resonance before $\mu \approx 6$ (phase II) and after $\mu \approx 16$ (phase IV). Panel B: The height of the peak in A, which is highest for phases (II and IV) due to coherence resonance. Panel C: Signal-to-noise ratio (SNR) computed with the time series for the mean membrane potential of E neurons. The highest values occur again for phases II and IV, and the minimum ones during the incoherent phases (I and III). Panels D, E and F: Same as in panels A, B and C, respectively, but for the time series of the fraction $\rho(t)$ of firing E neurons, which confirm the results on the left.

maximum peak at a well defined frequency emerges during the intermediate region (phase II), where such frequency increases from $6\,Hz$ to $25\,Hz$ —thus describing the spectrum of α, β and γ waves— and, finally (phase IV), this goes from $80\,Hz$ to $130\,Hz$ —corresponding to high γ and ultrafast oscillations. The same is confirmed by time series for the fraction $\rho(t)$ of firing E neurons in Fig. 4D. This picture becomes even more coherent and interesting when one realizes, as it turns out to be the case, and we develop it below, that the passage from one behavior to a contiguous qualitatively-different one is throughout a non-equilibrium phase transition. The system in this

way exhibits varied behavior with quite efficient features and great economy [5].

On the other hand, the maximum peaks in Fig. 4B are higher in the presence of coherence resonance, i.e., phases II and IV, than during the incoherent phases I (not shown since not a clear peak develops in fact here) and III (characterized by intermittent behavior between low frequency and high frequency oscillations which also does not show a clear peak in the power spectra). The behavior is similar for $\rho(t)$ in Fig. 4E. It also interests the μ variation of the signal-to-noise ratio (SNR) at the power spectra maximum peak, i.e., its height divided by the average in a small range around.

Even more clear than the spectra peaks, the SNR shows maxima if coherence occurs (II and IV) and goes to minima in the incoherent phases (I and III), as it is shown in Fig. 4C (where the SNR is computed in the power spectrum of the time series of the average membrane potential) and in Fig. 4F (where the SNR is computed in the power spectrum of the fraction $\rho(t)$ of firing E neurons). Specifically, the maximum coherence value is achieved in both cases around $\mu \simeq 1.3$ (within phase II) and for $\mu \gtrsim 20$ (within phase IV), and it is also noticeable that the SNR maximum, for both the global membrane potential and $\rho(t)$, is higher for phase IV than for phase II. Despite this, since the SNR decreases during phase II as μ increases and due to the features of the phase III, where also SNR is low, it is hard to precisely determine the transition point between phase II and III using the SNR.

The above suggests a great interest in characterizing the transition regions separating qualitatively different behaviors as one varies μ and I_0. Particularly, there is interest in the transition between phases III and IV. Fig. 4A, for instance, reveals that this is sharp, suggesting a thermodynamic-like discontinuous phase transition. To address this, during simulations we run our system during 10s for each μ value, as we varied adiabatically this parameter in geometric progression while keeping $I_0 = 0$. We retained the final state of all the neurons in each run to serve as the initial state for the run at the next noise value, which only differs in a small percentage from the previous one. Once the maximum μ is reached, the process is reverted, keeping again each final state as the initial one during this noise reduction process. The resulting hysteresis cycle around transitions III$\leftrightarrow$IV is shown in Fig. 5A, which confirms the discontinuous first-order-like nature of the phase transition. Such (even small) hysteresis seems to reflect that the frequency of the global oscillations is not well-defined in phase III; in fact, this shows no clear peak in the power spectra, and the maximum we use to compute hysteresis

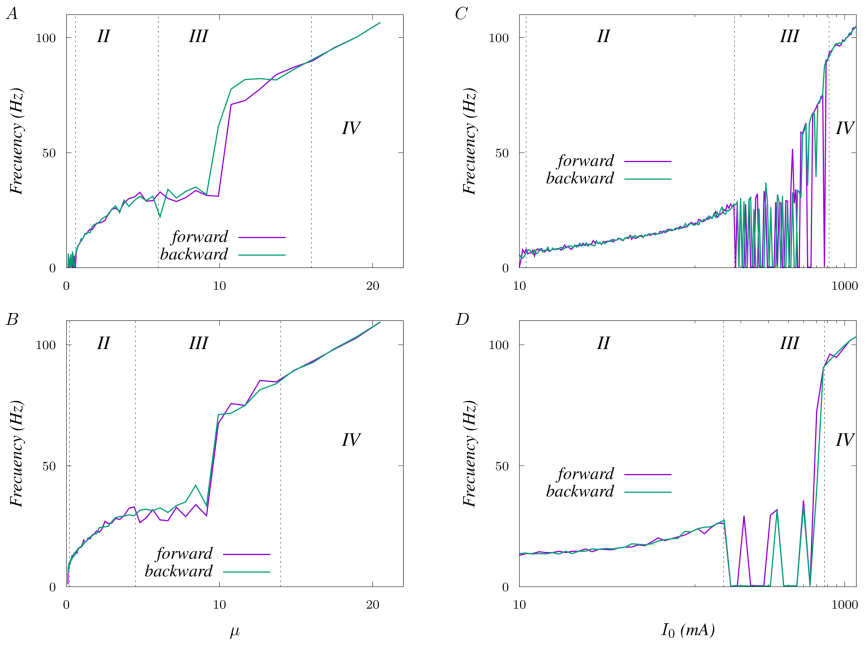

Figure 5: Study of hysteresis as a function of μ (left) and I_0 (right). Panel A: Frequency at which the maximum peak of the power spectra for the mean membrane potential of E neurons occurs (as μ is increased and decreased adiabatically with $I_0 = 0$). The two curves superimpose where the frequency is well defined. Panel B: The same but for $I_0 = 50$, confirming the phases in A, but shifted to the left. Panel C: The frequency, as computed in A, but as a function of the constant input I_0 for $\mu = 0.5$, which confirms the same phases and shows that $210 \leqslant I_0 \leqslant 750$ is a region of incoherent collective behavior in which frequency is not well-defined. Panel D: Same as in panel C but for $\mu = 1$ showing the same but with changes now shifted to the left relative to panel C because μ is now higher.

can depend on the run conditions and in the network size (small network size can make a metastable oscillatory state to jump quickly into the stable one). However, when the frequency is well-defined, the round-trip curves superimpose. We obtain similar results for $I_0 = 50$ in Fig. 5B, but with the phase changes somewhat shifted to the left.

The fact that our model shows the same qualitative behavior or phases within a wide ample range of I_0 values suggests that its behavior is robust to the type of input, and we confirmed this by moving I_0 adiabatically for $\mu = 0.5$ (Fig. 5C) and $\mu = 1$ (Fig. 5D). Note that phase I is not shown, since

for $\mu = 1$ the system is at phase II even for $I_0 = 10$, that phase III occurs for $180 \leq I_0 \leq 700$ and that, as expected, the phase changes are shifted to the left relative to Fig. 5C because μ is now higher. The conclusion is that the system is sensible to the total current arriving to the network but not to the type of input. In other words, increasing the noise and I_0 tends to increases the excitability of both neuron populations but the emergent behavior is rather due to the complex interplay between the activity of E and I populations.

Stochastic resonance as a detector of phase transitions in EEG activity

We also checked the case of a weak input $V_{\text{ext}} = d\,\sin(2\pi f t)$ with small d to the neural network, instead of $V_{\text{ext}} = 0$ as above. In general, even relatively small values of d induce a new maximum at frequency f in the power spectra, as shown in Fig. 6 (right column).

The emergent peak here —which happens to stand out more or less depending on the values for d and μ— reveals the existence of the so-called *stochastic resonance* (SR) phenomenon [13]. That is, the propagation of a weak signal is enhanced at certain intermediate level of noise while it is generally obscured at lower and higher levels of noise. The SNR in the power spectra consequently increases at those moderate values of the noise. As it was already shown [3], this is just a consequence of the great susceptibility the cooperative system exhibits in a region in which a phase transition occurs, so that it provides a simple method to detect changes of qualitative behavior in these types of systems.

A general evidence of SR phenomena in the system is illustrated in Fig. 7 for $I_0 = 0$, showing the *signal to noise ratio (SNR)* as a function of the noise level μ for both low-frequency ($\sim 4Hz$) and high-frequency ($\sim 40Hz$) inputs signals. In agreement with the interpretation of stochastic resonance in [3], here we observe how SR peaks develop around the phase transitions described above. For low-frequency signals (left graph) there are clear maximum at $\mu \approx 0.6$, 6 and 16 corresponding to the phase transitions I↔II, II↔III and III↔IV, respectively. The SNR also shows a peak for $\mu \approx 10$ which corresponds to the level of noise at which finite-size jumps between III↔IV occur in simulations. The emergence of this peak can be explained assuming that noise makes that these finite-size jumps of activity between both phases can be driven by the weak stimulus, so an amplification of the weak signal occurs at such noise level. Then, we expect that such peak will disappear as the network size is increased which will be an indication that

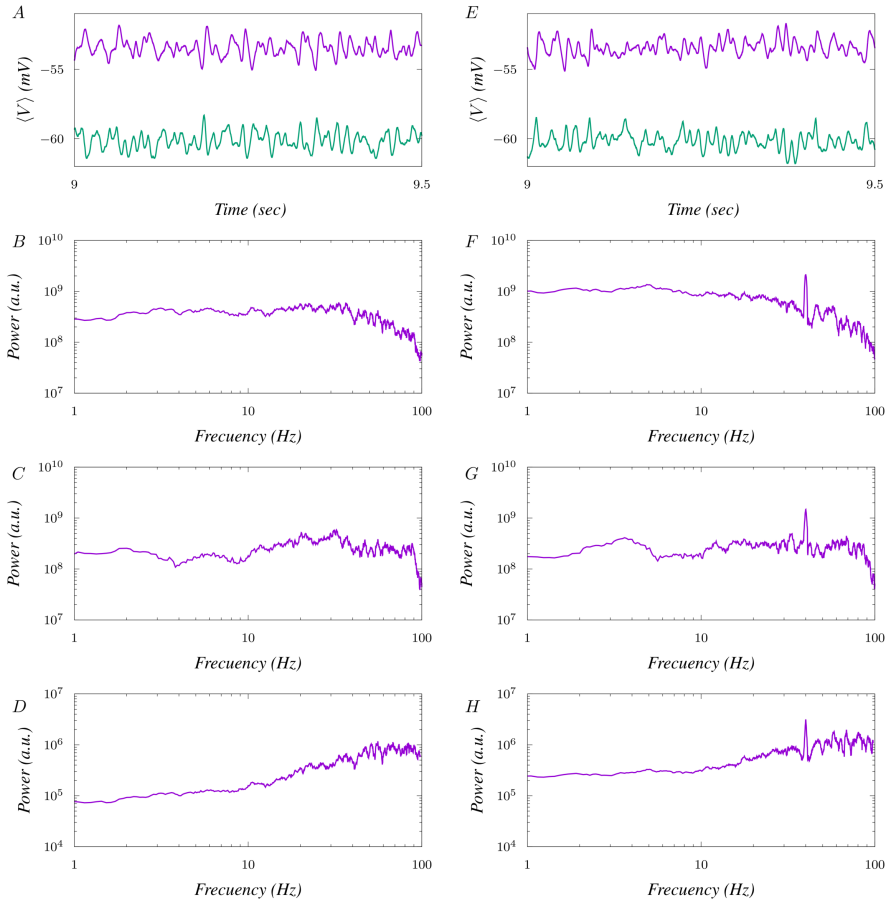

Figure 6: Case of $\mu = 10$ showing the effect of adding (right column) a small signal $V_{\rm ext} = d \sin 2\pi f t$ to each E neuron. The left column is for $d = 0$ while the right one is for $d = 25$ and $f = 40\,Hz$. Top panels show the mean membrane potential of E (green line) and I (violet line) neurons with (panel E) and without (panel A) the external signal. Panels B and F depict the corresponding (membrane potential) power spectra for the I neurons in both situations, and panels C and G show the same for E neurons. At the bottom, panels D and H illustrate the corresponding power spectra of the fraction $\rho(t)$ of firing E neurons. The signal only slightly modifies dynamics but a clear peak emerges at frequency f.

the transition III↔IV is of first-order type as simulations seams to indicate (see top graphs in Fig. 7). For high-frequency signals ($\sim 40Hz$), only the transitions II↔III and III↔IV are clearly marked by stochastic resonance peaks around $\mu \approx 6$ and 16, the first hardly distinguishable and the last

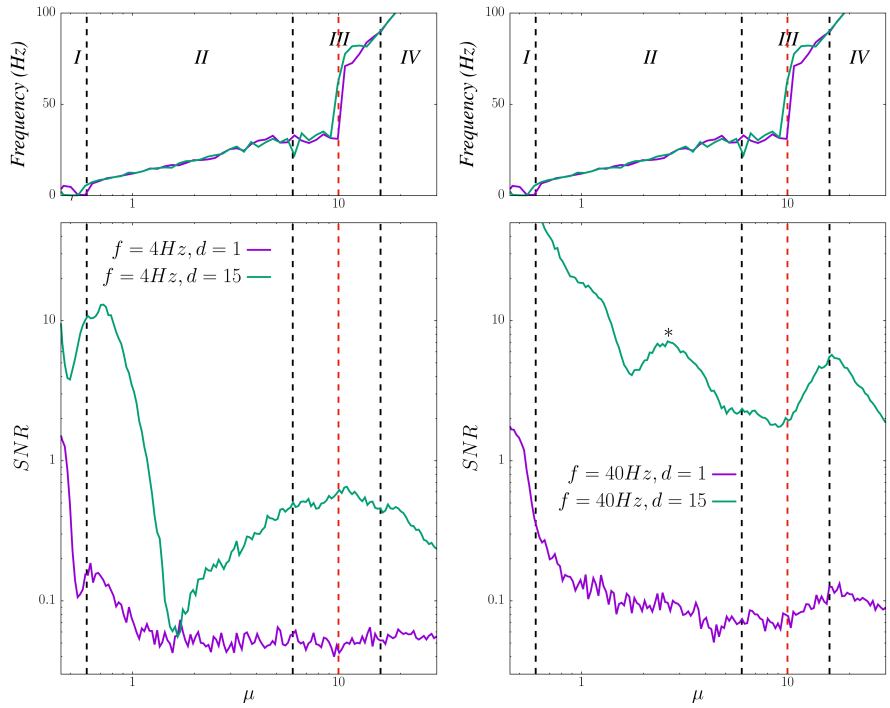

Figure 7: Emergence of *stochastic resonance* in the system in figure 1, for $I_0 = 0$, when a weak sinusoidal input V_{ext} of low frequency ($f \sim 4Hz$) (left graph) and high frequency ($f \sim 40Hz$) (right graph) affects each E neuron. SR peaks appear around the phase transition points (vertical dashed lines at $\mu = 0.6$, 6 and 16) depicted in the top panels. Note in the left graph that the jump corresponding to the change of behavior in simulations between phases IV and III (see top panel) appears around $\mu \approx 10$ (see red vertical dashed line) that coincides with the larger resonance peak for large level of noise. Secondary resonance peaks occur around this maximum for $\mu \approx 6$ and 16. In the right panel, however, such maximum does not show. Also, the low noise resonance peaks around $\mu \approx 0.6$ is neither appearing and the only ones are those around $\mu \approx 6$ (poorly seeing) and 16 (very clearly depicted). Different *SNR* curves here were obtained after averaging over 100 trials and computing the power spectra over a time series of $2^{18}ms$ for each trial.

one very clear. The peak around $\mu \approx 0.6$ is not appearing due to the fact that system oscillations at such level of noise at a natural frequency of alpha range around $10Hz$ or less, which is very small compared with the weak signal stimulation frequency ($40Hz$). This is incompatible with the emergence of the SR where the stimulation frequency must be very low compared with the intrinsic oscillation frequency of the system. Note that this impediment does not occur for the the resonance peak around $\mu = 16$ since for this case

the intrinsic oscillation frequency of the system is around $75Hz$ or larger which is bigger that the stimulation frequency of $40Hz$, so conditions for the emergence of SR still hold. The transition II$\leftrightarrow$III occurs around $\mu \approx 0.6$ with system oscillations of frequency around the stimulation frequency, so this is the reason why the SR peak around $\mu \approx 0.6$ is not so clearly depicted. Also remarkable in this high-frequency stimulation case is the presence of an additional resonance peak around $\mu \approx 2.5$ (marked with "*" in the figure) which corresponds with a range of frequencies$\sim 25 - 30Hz$, and it could indicate the exact limit between β (with intrinsic frequency between 12 to $30Hz$) and γ brain waves (with intrinsic frequency larger than $30Hz$) as experimental psychologists and neuroscientists have widely described (see for instance [23, 24, 25]). This overall behavior should also be discernible in actual EEG experiments.

Discussion

We here present an extension, and formalization according to recent familiar standards, of a model for the generation of brain α rhythms [10] which provides a simple and well-defined scenario also for other types of brain waves. In addition to signals from other neurons (V_{in}), and from outside the network —which are globally portrayed here as a Poisson noise (V_{noise}) which is characterized by the parameter μ— our model Eq. (1) includes a constant current I_0 and a small external input signal V_{ext}. Our main findings may be summarized as follows:

- Previous results [10] are confirmed using a more precise dynamics including a smaller time step during the model time integration. Contrary to [10] this fact results in a slightly lower but more precise degree of coherence, since we observed that large time step artificially increases the coherence (data not shown).

- In this way, we identify four different "phases" or qualitative types of dynamic behavior in the model. As μ is increased, this exhibits oscillations that are too weak in amplitude so that any coherence is precluded (phase I), a phase of coherence resonance (phase II), asynchrony within neuron's populations and incoherent behavior showing abrupt jumps in the corresponding frequency curves (phase III), and neuron population coherent behavior with a well-defined frequency again (phase IV).

- In phase II, our system precisely includes the frequency spectrum of α, β and low γ waves of actual EEG recordings, and phase IV covers the frequencies corresponding to high γ and ultrafast oscillations.
- The highest coherence resonance, as revealed by the power spectra peak and the corresponding SNR, is for phases II and IV, while the lowest one occurs in the incoherent phases I and III.
- The average amount of electrical impulses arriving to the network per unit of time —that we parametrize as μ— is essential to characterize the different phases, more than the nature, either constant or noisy, of the input.
- *Stochastic resonance* [3, 5] is revealed, e.g., by SNR, locating changes of qualitative behavior when the system receives a signal. We confirm that this fact may provide a powerful tool to investigate phase transitions in mammals and other brains using simple techniques such as EEG recordings or simple experiments as devised in [3].

The above picture indicates, on one hand, that a single unified mechanism can generate rhythms which are similar to the familiar brain rhythms, in the sense that we do not need a mechanism for alpha waves, another mechanism for beta waves, etc; the same mechanism explains different types of brain waves, and moreover we do not need additional assumptions concerning conduction times to explain different types of brain waves. On the other hand, it indicates that such waves are related to the general phenomena of non-equilibrium phase transitions, where a system is known to be highly susceptible, efficient and adaptable [12, 5]. This is compatible with specific mechanisms that might act during the generation of brain oscillations while cognitive functions occur. However, a one-to-one correspondence between different type of brain oscillations and cognitive functions cannot be established in fact, there are many more different cognitive processes than types of brain waves [26]. It seems sensible to assume that similar brain waves in the same frequency band can contribute to different cognitive functions depending on the particular brain area in which they originated and on their particular temporal features [26]. For example [27], while local synchronization during visual processing evolves in the γ range, synchronization between neighboring temporal and parietal cortex during multi-modal semantic processing may evolve in a lower β (12-18 Hz) range, and long range fronto-parietal interactions during working memory retention and mental imagery

in the θ (4-8 Hz) and α (8-12 Hz) ranges. That is, a relationship may exist between functional integration and synchronization frequency which could be due to conduction delays in long corticortical axons —up to several tens of ms for conduction distances of $\sim$10 mm— and convert γ to β oscillations (with cycle times ranging from 30 to 70 ms). The same process for more widely-dispersed interactions could produce activity in the active cortex in the α range (cycle time 77–125 ms) or even in the θ range. To our knowledge, however, these details have yet been poorly demonstrated and the argument requires that all axonal connections of a given network were approximately the same length, which is a too strong assumption for regions of arbitrary extension. In addition, electrical stimulation of V1 induces enhanced γ-band activity in V4, whereas V4 stimulation induces enhanced α-β-band activity in V1 [28], when it is suppossed that the conduction delays are approximately the same from V1 to V4 than from V4 to V1. Recognizing that the presence of conduction delays may importantly complicate the network dynamics [29], and that brain oscillations could be related to many biological oscillations [30] – as heart rate, heart rate variability, breathing frequencies, fluctuations in the BOLD signal, and others – our proposal does not require any hypothesis concerning conduction times or too speculative assumptions concerning the coupling of the brain activity with any type of body oscillations. From a different point of view, given the modular structure of the brain [31], we may imagine small networks with a great internal connectivity, each as ours here and perhaps in some of the dynamic phases we have described subject to an input. Furthermore, it is sensible to assume that, in a large region of interconnected neurons, an input from other modules will not affect all the neurons, since otherwise it might induce an anomalous high physiological level of activity. On the average, one should expect our parameter μ to be low and only high inputs eventually reaching small local regions. Within this scenario, our model suggests that large synchronized regions receive small inputs, and therefore will oscillate in the α regime, while small local synchronized regions receiving a large input will oscillate synchronously in the γ range. Our scenario is thus compatible with the one in [32].

Also, we mention that some authors associate consciousness with coherent γ oscillations in different parts of the brain, and thus explain episodes of attention [33]. In the light of our results, we can hypothesize that the transition III$\rightarrow$IV could be related to the emergence of awareness of memories associated with the modules that reach the corresponding input, a hypothesis that could be tested experimentally. In fact, we could include all the

40-70 Hz frequencies in phase IV choosing adequately model parameter values. In particular, our network model may easily involve a small random delay of small variance in all the connections, a topology different that the one in Fig. 1A, and/or vary the parameters of the EPSP and IPSP waves in Fig. 1B to achieve this. Other theories of consciousness, as the Integrated Information Theory [34] and its continuous dynamical system version [35] are also consistent with our scenario in which one may have two phases with very different levels of activity, both with a synchronicity that facilitates the communication with other mechanisms, and our phases II and IV would be equivalent to the "off" and "on" states in this theory.

In the present model the values of ratio η/ϵ, the refractory times and all other parameters like τ_1 and τ_2 have been chosen to properly reproduce a small module in a realistic way. We have checked, however, that the presented results and conclusions are robust against small variations of these parameters' values. In particular, the main conclusion of the present work, i.e. the existence of a unifying mechanism for the generations of oscillatory waves in the module as a function of the noisy input is not dependent on these parameters' variations.

The present model can be easily extended to other complex networks topologies including, e. g., scale-free and small-world features. Note, however, that such topologies in general involves several order of magnitude and therefore very large networks sizes, that as we have demonstrated is not a requirement for the emergence of the oscillatory behavior similar to brain waves reported in the present work. Both the scale-free and the small-world networks may be appropriate for the efficient transmission or diffusion of the waves to other brain areas but are not necessary here for the generation of the waves.

Acknowledgments

We acknowledge the Spanish Ministry for Science and Technology and the "Agencia Española de Investigación" (AEI) for financial support under grant FIS2017-84256-P (FEDER funds).

References

[1] V. M. Eguiluz, D. R. Chialvo, G. A. Cecchi, M. Baliki, and A. V. Apkarian. Scale-free brain functional networks. *Physical Review Letters* 94: 018102, 2005.

[2] J. Hesse and T. Gross. Self-organized criticality as a fundamental property of neural systems. *Frontiers in Systems Neuroscience* 8: 166, 2014.

[3] J. J. Torres and J. Marro. Brain performance versus phase transitions. *Scientific Reports* 5: 12216, 2015.

[4] L. Brochini, A. de Andrade Costa, M. Abadi, A. C. Roque, J. Stolfi and O. Kinouchi. Phase transitions and self-organized criticality in networks of stochastic spiking neurons. *Scientific Reports* 6: 35831, 2016.

[5] J. Marro and D. R. Chialvo, *La mente es crÃtica — Descubriendo la admirable complejidad del cerebro*, EUG (University of Granada Press), Granada, 2017 (an English new version of the contents of this book is now in progress).

[6] M. A. Muñoz. Colloquium: Criticality and dynamical scaling in living systems. *Review of Modern Physics* 90(3): 031001, 2018.

[7] L. Cocchi, L. L. Gollo, A. Zalesky, M. Breakspear. Criticality in the brain: A synthesis of neurobiology, models and cognition. *Progress in Neurobiology* 158: 132-152, 2017.

[8] L. L. Gollo. Coexistence of critical sensitivity and subcritical specificity can yield optimal population coding. *Journal of The Royal Society, Interface* 14(134): 20170207, 2017.

[9] S. Palva and J. Matias Palva. Roles of brain criticality and multiscale oscillations in temporal predictions for sensorimotor processing. *Trends in Neurosciences* 41(10): 729-743, 2018.

[10] F. H. Lopes da Silva, A. Hoeks, H. Smits, and L. H. Zetterberg. Model of brain rhythmic activity. *Kybernetik* 15(1):27-37, 1974.

[11] N. Dehghani, A. Peyrache, B. Telenczuk, M. Le Van Quyen, E. Halgren, S. S. Cash, N. G. Hatsopoulos and A. Destexhe Dynamic balance of excitation and inhibition in human and monkey neocortex. *Scientific Reports* 6: 23176, 2016.

[12] J. Marro and R. Dickman. *Nonequilibrium Phase Transitions in Lattice Models,* Cambridge University Press, Cambridge, 2005.

[13] L. Gammaitoni, P. Hänggi, P. Jung, and F. Marchesoni. Stochastic resonance. *Review of Modern Physics* 70: 223-287, 1998.

[14] T. Tömböl. Short neurons and their synaptic relations in the specific thalamic nuclei. *Brain Research* 3(4): 307-26, 1967.

[15] V. Braitenberg and A. Schüz. *Cortex: Statistics and Geometry of Neuronal Connectivity,* Springer, 1998.

[16] H. Markram, M. Toledo-Rodriguez, Y. Wang, A. Gupta, G. Silberberg, and C. Wu. Interneurons of the neocortical inhibitory system. *Nature Review of Neuroscience* 5(10): 793-807, 2004.

[17] M. Okun and I. Lampl. Balance of excitation and inhibition. *Scholarpedia* 4(8): 7467, 2009.

[18] L. F. Abbott. Lapicque's introduction of the integrate-and-fire model neuron (1907). *Brain Research Bulletin* 50(5-6): 303-304, 1999.

[19] E. R. Kandel, J.H. Schwartz and T. M. Jessell. *Principles of Neural Science,* McGraw-Hill, 2000.

[20] W. R. Levick and W. O. Williams. Maintained activity of lateral geniculate neurones in darkness. *Journal of Physiology* 170: 582-597, 1964.

[21] J. M. Fuster, A. Herz and O. D. Creutzfeldt. Interval analysis of cell discharge in spontaneous and optically modulated activity in the visual system. *Archives Italiennes de Biologie* 103(1): 159-177, 1965.

[22] Ch. Koch. *Biophysics of Computation: Information Processing in Single Neurons,* Oxford University Press, 1999.

[23] R. E. Dustman, R. S. Boswell and P. B. Porter. Beta brain waves as an index of alertness. *Science* 137(3529): 533-534, 1962.

[24] G. Buzsáki. *Rhythms of the Brain,* Oxford University Press, 2006.

[25] J. D. Kropotov. Beta Rhythms. *In: Quantitative EEG, Event-Related Potentials and Neurotherapy,* Academic Press, San Diego, 2009, 59-76, 2009.

[26] C. S. Herrmann, D. Strüber D, R. F. Helfrich and A. K. Engel. EEG oscillations: from correlation to causality. *International Journal of Psychophysiology* 103: 12-21, 2016.

[27] R. Miller. Theory of the normal waking eeg: From single neurones to waveforms in the alpha, beta and gamma frequency ranges. *International Journal of Psychophysiology* 64(1): 18-23, 2007.

[28] G. Michalareas, J. Vezoli, S. Pelt, J. Schoffelen, H. Kennedy and P. Fries. Alpha-beta and gamma rhythms subserve feedback and feedforward influences among human visual cortical areas. *Neuron* 89: 384-397, 2016.

[29] W. S. Lee, E. Ott and T. M. Antonsen. Large coupled oscillator systems with heterogeneous interaction delays. *Physical Review Letters* 103: 044101, 2009.

[30] W. Klimesch. The frequency architecture of brain and brain-body oscillations: An analysis. *European Journal of Neuroscience* 48(7): 2431-2453, 2018.

[31] E. Bullmore and O. Sporns. Complex brain networks: graph theoretical analysis of structural and functional systems. *Nature Reviews of Neuroscience* 10(3): 186-198, 2009.

[32] A. von Stein and J. Sarnthein. Different frequencies for different scales of cortical integration: from local gamma to long range alpha/theta synchronization. *International journal of psychophysiology* 38(3): 301-13, 2000.

[33] F, Crick and Ch. Koch. Towards a neurobiological theory of consciousness. *Seminars in the neurosciences* 2: 263-275, 1990.

[34] M. Oizumi, L. Albantakis and G. Tononi. From the phenomenology to the mechanisms of consciousness: Integrated information theory 3.0. *PLoS Computational Biology* 10(5): 1-25, 2014.

[35] F. J. Esteban, J. A. Galadí, J. A. Langa, J. R. Portillo and F. Soler-Toscano. Informational structures: A dynamical system approach for integrated information. *PLoS Computational Biology* 14(9): e1006154, 2018.